

# The topological structure of $SU(2)$ gluodynamics at $T > 0$ : an analysis using the Symanzik action and Neuberger overlap fermions

V. G. Bornyakov

*Institute for High Energy Physics, Protvino, 142281, Russia and  
Institute of Theoretical and Experimental Physics,  
B. Cheremushkinskaya 25, Moscow, 117259, Russia*

E. V. Lushevskaya, S. M. Morozov, and M. I. Polikarpov

*Institute of Theoretical and Experimental Physics,  
B. Cheremushkinskaya 25, Moscow, 117259, Russia*

E.-M. Ilgenfritz

*Institut für Physik, Karl-Franzens-Universität Graz,  
Universitätsplatz 5, A-8010 Graz, Austria and  
Humboldt-Universität zu Berlin, Institut für Physik,  
Newtonstrasse 15, 12489 Berlin, Germany*

M. Müller-Preussker

*Humboldt-Universität zu Berlin, Institut für Physik,  
Newtonstrasse 15, 12489 Berlin, Germany*

(Dated: February, 22, 2009)

We study  $SU(2)$  gluodynamics at finite temperature on both sides of the deconfining phase transition. We create the lattice ensembles using the tree-level tadpole-improved Symanzik action. The Neuberger overlap Dirac operator is used to determine the following three aspects of vacuum structure: (i) The topological susceptibility is evaluated at various temperatures across the phase transition, (ii) the overlap fermion spectral density is determined and found to depend on the Polyakov loop above the phase transition and (iii) the corresponding localization properties of low-lying eigenmodes are investigated. Finally, we compare with zero temperature results.

PACS numbers: 11.15.Ha, 12.38.Gc, 12.38.Aw

## I. INTRODUCTION

More than ten years ago, in a model generalizing random matrix theory, M. A. Stephanov [1] has built in the feature that in  $SU(3)$  gluodynamics above  $T_c$  the different Polyakov loop sectors should behave differently. In the sectors with complex-valued average Polyakov loop the chiral condensate was expected to turn to zero at a temperature  $T$  substantially higher than  $T_c$ , the deconfinement temperature. Prior to this paper, similar observations in quenched  $SU(3)$  lattice simulations had been reported by Chandrasekharan and Christ [2, 3]. For  $SU(2)$  lattice gluodynamics, where the Polyakov loop is real, it was predicted that the chiral condensate stays non-zero,  $\langle \bar{\psi}\psi \rangle \neq 0$ , for all temperatures  $T > T_c$  in the sector with a negative average Polyakov loop,  $L < 0$ .

Simulating quenched  $SU(3)$ , Gattringer *et al.* [4] came to a different result. These authors used the spectral gap in the spectrum of the Dirac operator as an order parameter for the restoration of chiral symmetry. It was found that the spectral gap opens up at one single temperature  $T = T_c$  in all three  $Z_3$  sectors.

In  $SU(2)$  gluodynamics this question has not been clarified before. In this case the behavior may be completely different. Indeed, there are pure vacuum gauge field configurations with  $L = 1$  for which the Dirac operator has trivial zero modes for periodic fermionic boundary conditions. Contrary to  $SU(3)$ , for  $SU(2)$  (as well as for any even number of colors) through a non-periodic  $Z(2)$  gauge transformation with  $-\mathbf{I} \in Z(2)$  this is equivalent to the existence of zero modes for antiperiodic fermion boundary conditions in the case of  $L = -1$ . In the light of this argument, we shall examine whether Stephanov's prediction for the Dirac spectrum remains valid in the case of  $SU(2)$  gluodynamics in the deconfined phase. Preliminary results were presented in [5].

We base our study on Neuberger's overlap Dirac operator [6]. Our interest will be concentrated on its spectrum, how it is related to the average Polyakov loop, and how this is reflected by the localization properties of the modes in various parts of the spectrum. Because of the index theorem [7, 8], the zero modes give us easy access to the topological charge  $Q$  of the lattice configurations, which is sufficient to calculate the topological susceptibility. In our present work, in contrast to Ref. [9], we will not exploit the capability of the overlap Dirac operator to provide us with a tool to analyse the topological charge density [10].

A first study of the overlap Dirac operator  $D_{ov}$  in  $SU(2)$  gluodynamics at finite temperature has been undertaken by the authors of Ref. [11]. They have used the usual Wilson gauge field action which means that for the same lattice spacing their configurations are substantially more rough than ours. We compare our results with theirs at several places in the following.

The outline of the paper is as follows. In Sect. II we explain the action used and quote the ensembles investigated. In Sect. III we discuss the structure and handling of Neuberger's overlap operator. In Sect. IV we report about the  $T$ -dependence of the topological susceptibility and in Sect. V about the temperature *and* Polyakov loop dependence of the spectral density. In Sect. VI we define the spectral gap as a deconfinement order parameter. In Sect. VII the localization properties of the Dirac eigenfunctions are described in the confined and deconfined phase, and the dependence on the Polyakov loop is pointed out for the latter. In Sect. VIII we assess the volume and lattice-spacing dependence of all discussed observables. In a separate Sect. IX we consider an exceptional, relatively well separated part of the non-zero modes with very small eigenvalues. After a discussion of topological susceptibility, spectral density and localization for the case of zero temperature in Sect. X, a summary is given in Sect. XI.

## II. THE IMPROVED ACTION

In an initial study, partly reported at Lattice 2007 [5], we have analyzed ensembles of  $O(100)$  statistically independent  $SU(2)$  configurations, generated in the quenched approximation with the tadpole improved Symanzik action on lattices of size  $20^3 \times 6$ . This action is known to suppress dislocations, that would lead to unphysical near-to-zero modes of the Wilson-Dirac operator. These are highly unwanted because they lead to difficulties to choose a uniform  $\rho$  parameter (see below). The form of the action is :

$$S = \beta_{\text{imp}} \sum_{pl} S_{pl} - \frac{\beta_{\text{imp}}}{20u_0^2} \sum_{rt} S_{rt}, \quad (1)$$

where  $S_{pl}$  and  $S_{rt}$  denote the plaquette and  $1 \times 2$  rectangular loop terms in the action,  $S_{pl,rt} = (1/2) \text{Tr} (1 - U_{pl,rt})$ . The factor  $u_0 = (W_{1 \times 1})^{1/4}$  is the *input* tadpole factor. It is selfconsistently determined from  $W_{1 \times 1} = \langle (1/2) \text{Tr} U_{pl} \rangle$  computed at zero temperature [12]. The deconfining phase transition, which is of second order for  $SU(2)$  gluodynamics, is not easy to locate precisely [13] because of strong finite volume effects. We have approximately determined the critical  $\beta_{\text{imp},c} = 3.248(2)$  on lattices of size  $20^3 \times 6$ , *i.e.* for  $N_\tau = 6$ . This corresponds to a ratio  $T_c/\sqrt{\sigma} = 0.71(2)$  [9].

To check for finite spatial volume effects, we made additional simulations also on  $24^3 \times 6$  lattices as well as on smaller lattices  $16^3 \times 6$  and  $12^3 \times 6$ . Furthermore, we also checked whether our results are close to the continuum limit. For this check we have simulated the neighbourhood of the transition on a finer lattice, with  $N_\tau = 8$ , for which a critical  $\beta_{\text{imp},c} = 3.425(5)$  was found in simulations on lattices with a spatial extent  $N_s = 24$ . For these  $24^3 \times 8$  lattices our actual measurements were performed only at one temperature very close to  $T_c$  in the confinement phase.

The parameters of the lattices used in this study and the respective statistics are reported in Table I. The lattice scale  $a$  needed to compute  $T/T_c$  has been obtained by interpolating the results of Ref. [12].

For a comparison with zero temperature, we have made simulations on symmetric lattices. Respective parameters are also given in Table I. At zero temperature the inverse coupling was chosen according to the lattice size such that the physical size was kept approximately fixed and equal to  $(1.4 \text{ fm})^4$ .

$N_\tau \times N_s^3$	$\beta_{imp}$	$T/T_c$	$\#conf.$	$N_{modes}$
$6 \times 12^3$	3.20	0.91	998, 910	20
$6 \times 12^3$	3.23	0.97	893, 900	20
$6 \times 16^3$	3.20	0.91	482, 517	30
$6 \times 16^3$	3.23	0.97	246, 262	50
$6 \times 16^3$	3.325	1.15	183, 215	30
$6 \times 16^3$	3.50	1.55	308, 96	50
$6 \times 20^3$	3.20	0.91	48, 49	50
$6 \times 20^3$	3.23	0.97	152, 147	50
$6 \times 20^3$	3.275	1.05	89, 102	50
$6 \times 20^3$	3.30	1.10	42, 56	50
$6 \times 20^3$	3.325	1.15	101, 98	50
$6 \times 20^3$	3.35	1.20	123, 75	50
$6 \times 20^3$	3.40	1.31	148, 0	50
$6 \times 20^3$	3.50	1.55	89, 98	50
$6 \times 20^3$	3.64	2.00	99, 98	50
$6 \times 24^3$	3.23	0.97	55, 41	45
$6 \times 24^3$	3.325	1.15	115, 50	45
$6 \times 24^3$	3.35	1.20	46, 00	45
$6 \times 24^3$	3.50	1.55	78, 81	45
$8 \times 24^3$	3.42	0.99	28, 31	25
$10 \times 10^3$	3.096	0	200	40
$12 \times 12^3$	3.196	0	100	40
$14 \times 14^3$	3.281	0	100	40
$16 \times 16^3$	3.3555	0	100	40
$20 \times 20^3$	3.5	0	99	20

TABLE I: The simulations details. The fourth column shows numbers of configurations with  $L >$  and  $L < 0$  separately where the two states can be distinguished.

### III. THE MASSLESS OVERLAP DIRAC OPERATOR

The massless overlap Dirac operator has the form [6]

$$D_{ov} = \frac{\rho}{a} \left( 1 + D_W / \sqrt{D_W^\dagger D_W} \right), \quad (2)$$

where  $D_W = M - \rho/a$  is the Wilson-Dirac operator with a negative mass term  $\rho/a$ ,  $M$  is the Wilson hopping term with  $r = 1$ , and  $a$  is the lattice spacing. With respect to the locality property of the overlap operator the optimal value of the  $\rho$  parameter is found to be  $\rho = 1.4$  also for the lattice ensembles under investigation. Standard boundary conditions, anti-periodic in time and periodic in spatial directions, are imposed to the fermionic field and the overlap Dirac operator.

In order to compute the sign function in

$$D_W / \sqrt{D_W^\dagger D_W} = \gamma_5 \text{sign}(H_W), \quad (3)$$

where  $H_W = \gamma_5 D_W$  is the *hermitian* Wilson-Dirac operator, we have used the minmax polynomial approximation. More precisely, we have treated 20 to 50 lowest Wilson-Dirac eigenmodes explicitly and used the polynomial approximation in the subspace orthogonal to these lowest Wilson-Dirac eigenmodes. The overlap Dirac operator  $D_{ov}$  constructed this way preserves the chiral symmetry

even on a lattice with finite  $a$  and allows to exploit the perfect chiral properties of the emerging Dirac overlap eigenmodes. The overlap operator will be called  $D$  in the following and replaces the continuum Dirac operator  $D = D_\mu \gamma_\mu$ , where  $D_\mu = \partial_\mu - igA_\mu$  is the covariant partial derivative with the gauge field background  $A_\mu$ .

#### IV. THE TOPOLOGICAL SUSCEPTIBILITY $\chi_{top}(T)$

We solved the Dirac equation numerically finding its eigensystem

$$D \psi_n = \lambda_n \psi_n, \quad (4)$$

restricted to the 50 lowest eigenvectors by means of ARPACK [14]. They are perfectly located on the Ginsparg-Wilson circle. By stereographic projection they are mapped to the imaginary axis. These purely imaginary eigenvalues  $\lambda_{\text{impr}}$  are then representing the  $O(a)$  improved overlap Dirac operator. The spectral densities presented later are distributions with respect to the imaginary part of  $\lambda_{\text{impr}}$ .

Our first task was the search for exact zero modes. Their number is related to the total topological charge  $Q_{top}$  of the lattice configuration through the index theorem [7, 8] :

$$Q_{top} \equiv Q_{index} = N_- - N_+, \quad (5)$$

where  $N_-$  and  $N_+$  are the numbers of zero modes  $\psi_{i0}$  with negative and positive chirality,  $\psi_{i0}^\dagger \gamma_5 \psi_{i0} = \pm 1$ , respectively. Actually, we found only configurations with  $N_+$  or  $N_-$  or both vanishing. For the lattice ensembles the average topological charge  $\langle Q_{top} \rangle$  should vanish, while the second moment  $\langle Q_{top}^2 \rangle$  measures the strength of global topological fluctuations. The topological susceptibility is measured as

$$\chi_{top} \equiv \frac{\langle Q_{top}^2 \rangle}{V}, \quad (6)$$

where  $V$  is the four-dimensional lattice volume in physical units. In Fig. 1 (left) we show a histogram of the topological charge in the confinement phase, close to the transition. Fig. 1 (right) shows the corresponding histogram for a temperature higher up in the deconfinement phase. The histogram in the confinement phase can be approximately fitted by a Gaussian distribution, in the deconfinement phase the Gaussian fit is of more poor quality. Let us now discuss the topological susceptibility as function of temperature. In Fig. 2 (left) we show the topological susceptibility  $\chi_{top}$  separately for the positive ( $L > 0$ ) and the negative Polyakov loop sector ( $L < 0$ ) over the full temperature range. At temperatures  $T \leq 1.31 T_c$  we have obtained both sectors in the course of the usual Monte Carlo sampling. Flips between the sectors happened even at  $T > T_c$  due to finiteness of our volume. For  $T = 1.55 T_c$  and  $2.0 T_c$  we have not observed such flips and stayed within the  $L > 0$  sector. We then generated configurations for the  $L < 0$  sector in the following way. We applied a flip transformation changing the sign of the Polyakov loop to an equilibrium configuration with  $L > 0$  and then used the Monte Carlo algorithm to produce a necessary number of configurations for the other sector. No flips back to the  $L > 0$  sector have been observed during these runs. Taking all temperatures into account, there is no systematic influence of the sign of the Polyakov loop or, what is equivalent, of the type of temporal boundary conditions, on the topological susceptibility. This conforms to the observation in Ref. [15], for quenched  $SU(3)$  configurations at  $T = 0$  selected to have topological charge  $Q = \pm 1$ , that the content of zero modes does not change with a continuous, complex-valued factor used to implement non-trivial temporal boundary conditions in the Dirac operator [31].

The measurements for the two signs of the Polyakov loop agree with each other at all  $T$  within two standard deviations. In Fig. 2 (right) we compare our final averages for  $\chi_{top}(T)$ , which include for  $T < T_c$  all configurations and for  $T > T_c$  only the subsample with  $L > 0$ , with the results of Alles *et al.* [16] [32]. These authors have presented the values of  $10^{-4} \times \chi_{top}/\Lambda_L^4$  for various values of  $\beta$  for Wilson's action representing different temperatures. We took  $\Lambda_L = 14.15(42)$  MeV [16] and extracted their susceptibility values  $\chi_{top}(T)$  from these data. The topological susceptibility is slowly decreasing with increasing temperature for both sets of data. Notice that the overlap definition of  $Q$  results in a

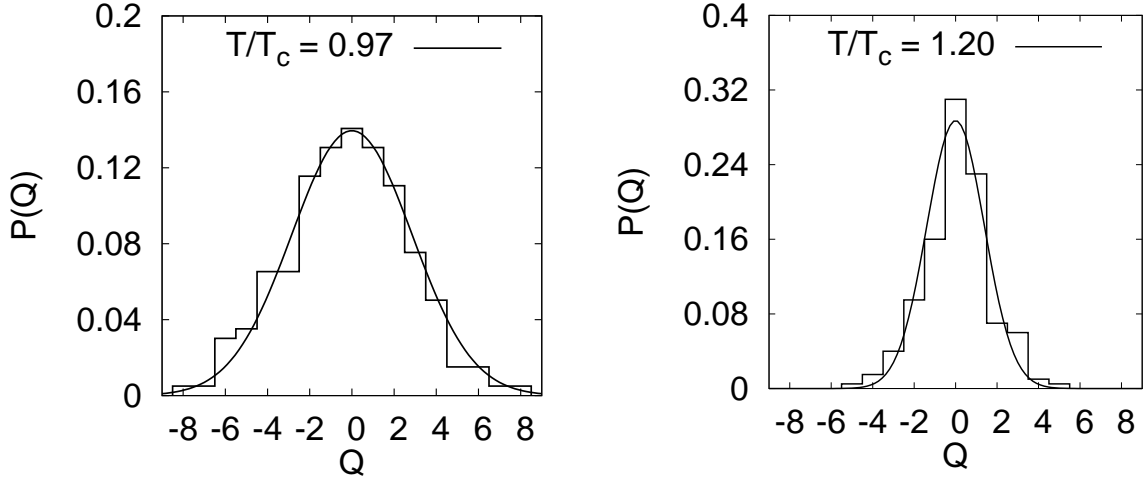


FIG. 1: Probability distributions of the topological charge  $Q$  for two temperatures below and above  $T_c$  on the  $20^3 \times 6$  lattice.

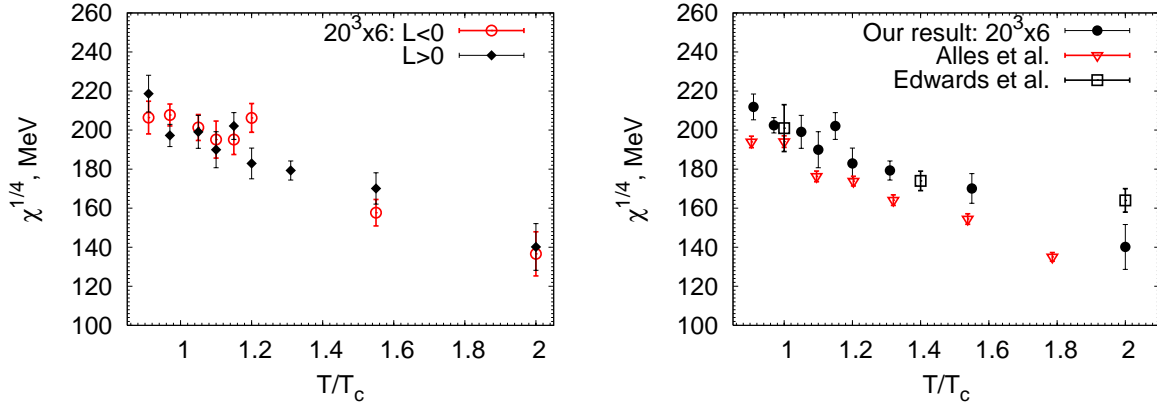


FIG. 2: The fourth root of the topological susceptibility  $\chi_{top}$  as function of  $T$  on the  $20^3 \times 6$  lattice. Left: separately for  $L > 0$  and  $L < 0$ . Right: comparison of our final result with that of Alles et al. [16] and Edwards et al. [11].

systematically higher susceptibility than the improved field theoretic definition employed by the Pisa group. Additionally we show results obtained in Ref. [11]. We took the data for the topological charge from their Table IV for temperatures  $T/T_c = 1.0, 1.4, 2.0$  and computed the respective susceptibilities. Statistical errors were computed by the bootstrap method. One can see that the results from Ref. [11] agree well with ours for  $T/T_c = 1$  and  $T/T_c = 1.4$  but slightly disagree for  $T/T_c = 2.0$ .

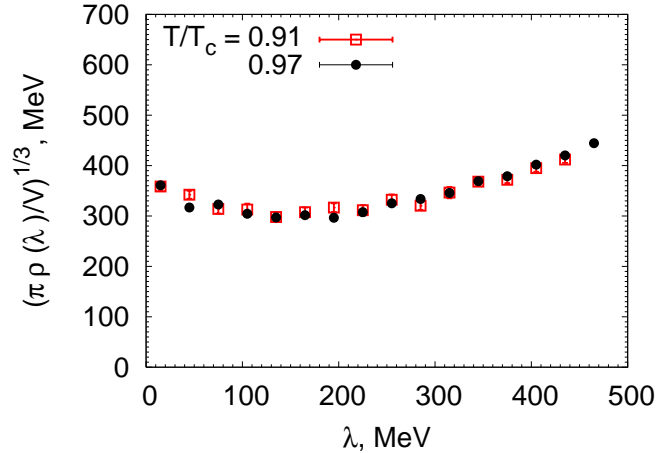


FIG. 3: The third root  $(\pi\rho(\lambda)/V)^{1/3}$  of the spectral density of non-zero eigenmodes of the overlap Dirac operator (at  $\lambda = 0$  approaching the third root of the quark condensate) is shown for two temperatures  $T < T_c$  as measured on the  $20^3 \times 6$  lattice. The modes are counted with a bin size of 30 MeV.

### V. THE SPECTRAL DENSITY AND CHIRAL SYMMETRY RESTORATION IN DIFFERENT $Z_2$ SECTORS

The chiral condensate  $\langle\bar{\psi}\psi\rangle$  is related to the density  $\rho(\lambda)$  of the non-zero eigenvalues  $\lambda$  at  $\lambda \rightarrow 0$  via the Banks-Casher [17] relation:

$$\langle\bar{\psi}\psi\rangle = - \lim_{\lambda \rightarrow 0} \lim_{m \rightarrow 0} \lim_{V \rightarrow \infty} \frac{\pi\rho(\lambda)}{V}. \quad (7)$$

The non-zero modes are globally non-chiral, but still *locally chiral* over a wide part of the spectrum, and their pseudoscalar density is known to be correlated with lumps of the topological charge density [18]. In the chirally broken phase the required limit (7) of  $\rho(\lambda)$  is non-vanishing at  $\lambda = 0$  [17]. In the chirally symmetric phase we expected vanishing  $\rho(\lambda) = 0$  in a finite region around the origin, in other words, that the spectrum develops a gap. It cannot be excluded that the gap (an operative definition is given below) tends to zero in the infinite-volume limit while the spectral density *at zero* remains vanishing,  $\rho(\lambda = 0) = 0$ . For the confinement (chirally broken) phase we find indeed that the spectral density in physical units is practically  $T$  independent and slightly increasing towards  $\lambda = 0$ . This can be seen in Fig. 3 where the third root  $(\pi\rho(\lambda)/V)^{1/3}$  of the spectral density is shown. At  $\lambda = 0$  it should approach the third root of the quark condensate.

The eigenvalue density is defined as

$$\rho(\lambda) = \lim_{\Delta\lambda \rightarrow 0} \frac{\langle N(\lambda, \Delta\lambda) \rangle}{\Delta\lambda}, \quad (8)$$

where  $N(\lambda, \Delta\lambda)$  counts the number of eigenvalues per configuration falling into the bin interval  $[\lambda - \Delta\lambda/2, \lambda + \Delta\lambda/2]$ . The averaging over all configurations available is denoted by  $\langle \dots \rangle$ . In practice we have chosen a finite bin size  $\Delta\lambda$  that is mentioned in each case.

We shall note that in the confinement phase, comparing results for configurations with average Polyakov loop  $L > 0$  and  $L < 0$ , we found at low  $\lambda$  the quantity  $(\pi\rho(\lambda)/V)^{1/3}$  to be  $50 \sim 70$  MeV higher for the negative Polyakov loop sector. We observed that this difference comes mostly from configurations with large  $|L|$ . This observation leads us to believe that such difference disappears in the thermodynamic limit since it is known that  $|L| \rightarrow 0$  in this limit.

For the deconfinement phase, when we take only configurations with an average Polyakov loop  $L > 0$ , the left panel of Fig. 4 shows that  $\rho(\lambda)$  non-uniformly decreases with increasing temperature,

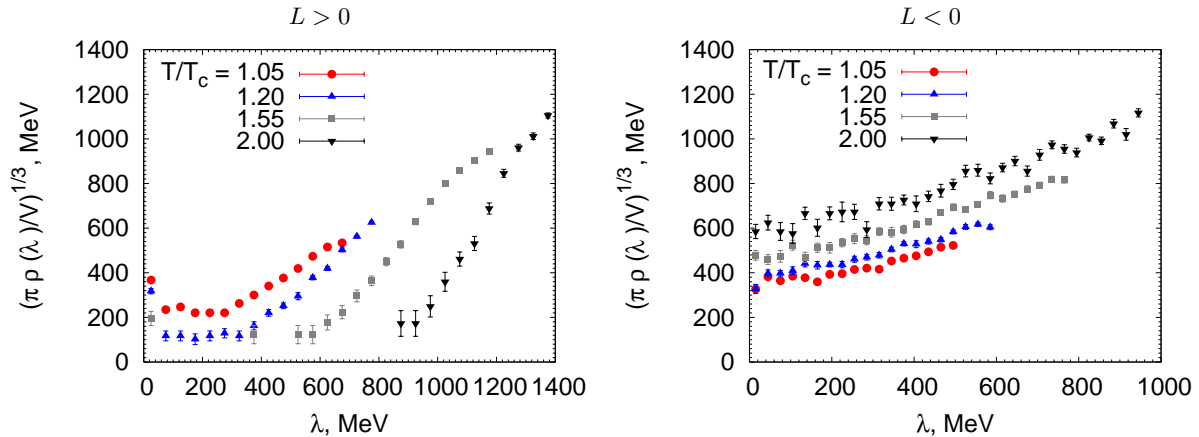


FIG. 4: The third root  $(\pi\rho(\lambda)/V)^{1/3}$  of the spectral density of non-zero eigenmodes of the overlap Dirac operator shown for 4 temperatures  $T > T_c$  as measured on a  $20^3 \times 6$  lattice, evaluated separately according to the sign of the averaged Polyakov loop:  $L > 0$  (left) and  $L < 0$  (right). The modes are counted for  $L > 0$  with a bin size of 50 MeV, for  $L < 0$  with a bin size of 30 MeV.

indicating the decrease of the quark condensate until a gap in the spectrum opens at  $T/T_c = 1.55$  and gets wider at  $T/T_c = 2$ . This does not completely agree with our expectation above. The gap, when it finally opens (for the  $L > 0$  sector) at  $T/T_c \approx 1.5$  needs a careful investigation in the infinite-volume limit. For configurations with  $L < 0$  the right panel of Fig. 4 shows that the third root of  $\pi\rho(\lambda)/V$  at low  $\lambda$  stays non-zero and even grows with increasing temperature. We checked that decreasing of the bin size down to 10 MeV does not uncover any gaps in the spectrum for  $L < 0$ .

For the temperatures above  $T_c$  in the sector with  $L > 0$ , in the interval  $\lambda \lesssim 50$  MeV we observe a particular enhancement in the spectrum of non-zero modes, that monotonously decreases with rising temperature. We will refer to these modes as “near-zero modes”. A similar observation has been made by Edwards *et al.* [11] for quenched configurations generated with the Wilson action. The fact that it reappears with the improved gauge action strongly hints that it is not a lattice artefact. The ensemble average of the lowest-lying one of these non-zero eigenvalues seems to be a natural definition of the spectral gap (see Sect. VI). The presence of the spectral enhancement, however, suggests a special, more careful analysis with respect to its origin that will be given in Sect. IX and will result in an alternative definition of the spectral gap.

The sector with  $L > 0$  plays a particular role because, as our results indicate in agreement with model considerations of Ref. [1], in this sector, together with the standard antiperiodic boundary conditions for fermions, chiral symmetry can be restored at sufficiently high temperature. We will furthermore see on the opposite that for the sector  $L < 0$ , with antiperiodic boundary conditions kept, chiral symmetry is not restored in the sense of the Banks-Casher relation.

However, with dynamical fermions included the sector with  $L > 0$  is the dynamically chosen sector in the high-temperature phase. For quenched configurations, when the fermionic boundary conditions can be changed at will from antiperiodic to periodic boundary conditions in time, the role of the sectors  $L > 0$  and  $L < 0$  is simultaneously interchanged.

## VI. THE SPECTRAL GAP

The spectral gap  $g_\lambda$  has been defined as the ensemble average of the smallest non-zero eigenvalue. In Ref. [4] Gatringer *et al.* have shown for  $SU(3)$  gluodynamics that the gap, as a function of temperature, has a different magnitude but a similar behavior for the real and both complex sectors (defined according to the complex phase of the averaged Polyakov loop). The phase transition – defined by the respective  $g_\lambda$  becoming non-zero – occurs at the same  $T_c$ . With increasing lattice volume the

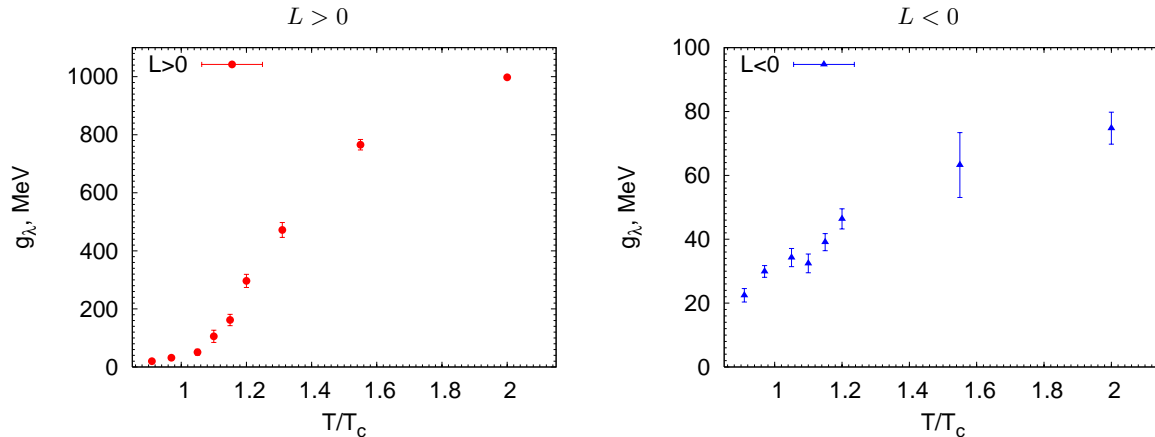


FIG. 5: The spectral gap for  $SU(2)$  lattice gauge theory as function of temperature, evaluated separately according to the sign of the averaged Polyakov loop on a  $20^3 \times 6$  lattice,  $L > 0$  (left) and  $L < 0$  (right). Notice the scales for the gap differing by a factor 10.

gap  $g_\lambda$  at each temperature  $T > T_c$  has the tendency to decrease, but this decrease seemed to stop at a finite limit. The infinite-volume limit of the gap in the three sectors has not yet been carefully analysed.

$SU(2)$  gluodynamics has only two sectors in the deconfinement phase, distinguished by the sign of the (real-valued) averaged Polyakov loop. We show in Fig. 5 (left) a clearly defined and rapidly growing gap  $g_\lambda$  for configurations with  $L > 0$ , whereas for configurations with  $L < 0$  the gap remains very small up to temperatures several times higher than  $T_c$ , as can be seen from the right panel of Fig. 5.

Our data presented in section IX (see Fig. 17(right)) strongly suggest that the small gap for  $L < 0$  is a pure finite-volume effect and vanishes in the limit of spatial  $V_3 \rightarrow \infty$ .

Physically more important in the light of our expectations would be to prove that the gap for  $L > 0$  – although also decreasing with increasing volume – has a finite limit at infinite volume. We postpone the discussion of this question to Sect. IX. Although the separation of the near-zero modes from the definition of the gap, that we will discuss there, will make the existence of a finite gap for all temperatures above  $T_c$  and for all available volumes obvious, a real infinite-volume limit of the gap  $g_\lambda$  has still to be explored.

## VII. LOCALIZATION IN DIFFERENT PARTS OF THE SPECTRUM

The scalar density of an eigenmode  $\psi_\lambda(x)$  corresponding to an eigenvalue  $\lambda$  is denoted as  $s_\lambda(x) = \psi_\lambda^\dagger(x)\psi_\lambda(x)$ , such that  $\sum_x s_\lambda(x) = 1$  by virtue of normalization. The inverse participation ratio (IPR)  $I_\lambda$  is the natural measure of the localization. For any finite volume  $V$  it is defined by

$$I_\lambda = V \sum_x s_\lambda^2(x). \quad (9)$$

The IPR characterizes the inverse volume fraction of sites forming the support of  $s_\lambda(x) = \psi_\lambda^\dagger(x)\psi_\lambda(x)$ . Its value is equal to the volume  $V$  for modes which are localized on a site, scales with  $V$  if it is localized on a finite number of lattice sites and is independent of the volume if its localization volume grows with the lattice volume. For  $T = 0$  the localization of overlap eigenmodes has been first investigated in Refs. [18, 19, 20, 21], for  $T \neq 0$  in Ref. [22, 23]. With a chirally improved Dirac operator, the localization properties have been investigated in detail earlier by Gattringer et al., for quenched  $SU(3)$  Yang-Mills theory at  $T = 0$  in Ref. [24] and for finite temperature in Ref. [25]. The localization



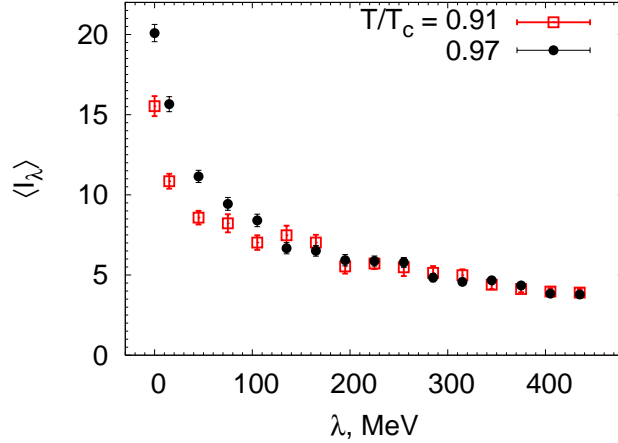


FIG. 6: The IPR averaged over zero modes and over subsequent spectral bins of width 30 MeV for two temperatures  $T < T_c$  on the lattice  $20^3 \times 6$ .

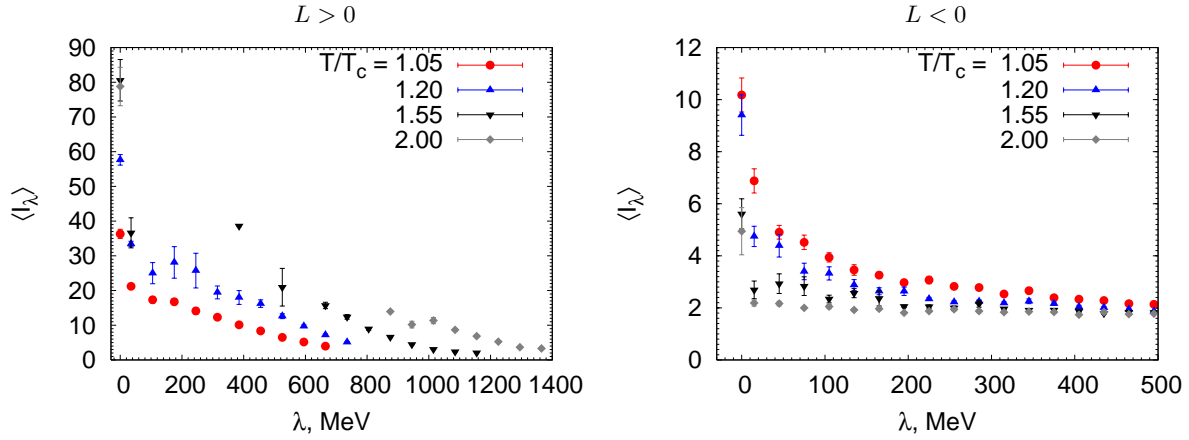


FIG. 7: The IPR averaged over zero modes and over subsequent spectral bins of width 70 MeV (left) and 30 MeV (right), separated according to the sign of the averaged Polyakov loop  $L > 0$  (left) and  $L < 0$  (right). Results are shown for four temperatures  $T > T_c$  on the lattice  $20^3 \times 6$ .

properties and their change with temperature are surprisingly similar for  $SU(3)$  and  $SU(2)$ . This applies to the overlap operator as well as to the chirally improved Dirac operator.

In the following figures the IPR are shown at  $\lambda = 0$  averaged over the zero modes, followed by the IPR averaged over the subsequent bins of non-zero modes. From Fig. 6 we conclude that for the temperature near but below  $T_c$  the IPR (localization) increases with decreasing eigenvalue, more or less in a monotonous fashion. There is no clear mobility edge. The zero modes are even more localized exceeding the first bin by  $\approx 50\%$ . Thus, out of the low-lying modes, the higher ones are continuously less localized. We found that at these temperatures for configurations with large in absolute value negative Polyakov loop,  $L < 0$ , the modes are less localized by a factor  $2 \sim 3$ . Again, as for  $\rho(\lambda)$ , this difference should disappear in the thermodynamic limit.

In Fig. 7 (left) we show for  $L > 0$  that with increasing temperature in the deconfinement phase the average IPR within the respective eigenvalue bins is increasing. With increasing temperature, the effect moves to higher and higher eigenvalues  $\lambda$ . This can be considered as a mobility edge moving, together with the gap, to larger  $\lambda$  in the deconfinement phase for  $L > 0$ . In the negative Polyakov loop sector the IPR is taking values at a much lower level. The temperature dependence at fixed  $\lambda$

is reverse compared to the  $L > 0$  sector, and the temperature dependence becomes stronger towards small  $\lambda$ . The spreading of the IPR values with respect to temperature is almost twice as large for zero modes compared to the smallest non-zero modes.

### VIII. FINITE VOLUME AND FINITE LATTICE SPACING EFFECTS ON TOPOLOGICAL SUSCEPTIBILITY, SPECTRAL DENSITY AND LOCALIZATION

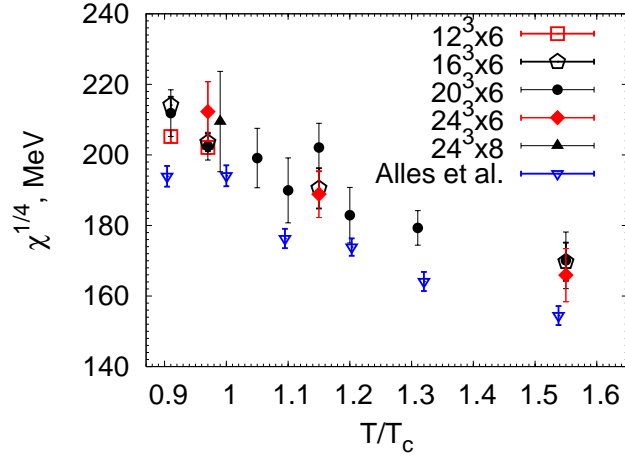


FIG. 8: The fourth root of the topological susceptibility  $\chi_{top}$  as function of  $T$  on  $12^3 \times 6$ ,  $16^3 \times 6$ ,  $20^3 \times 6$ ,  $24^3 \times 6$  and on  $24^3 \times 8$  lattices compared with the results of Ref. [16].

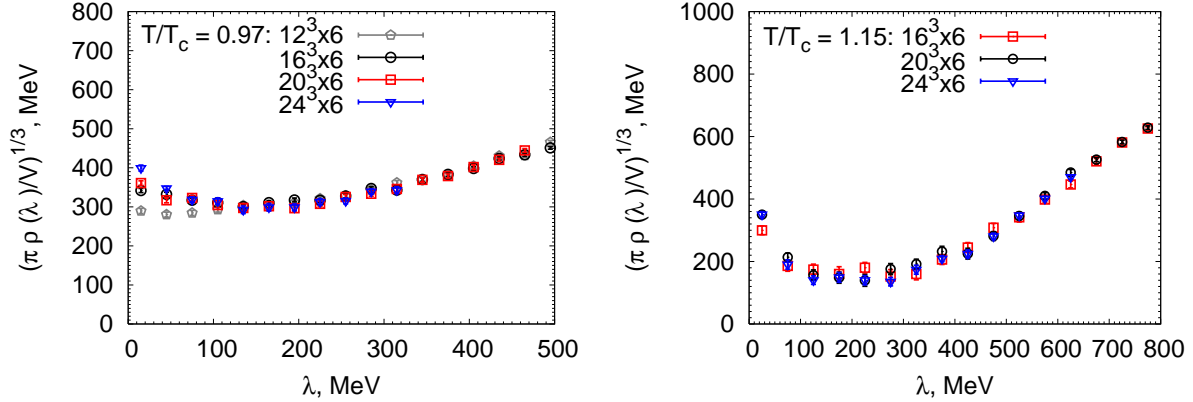


FIG. 9: The volume dependence of the third root of the averaged spectral density of non-zero eigenmodes of the overlap Dirac operator at  $T = 0.97 T_c$  (left) and  $T = 1.15 T_c$  (right). While  $N_\tau = 6$  in all cases, we compare four spatial lattice sizes with  $N_s = 12, 16, 20$  and  $24$  below  $T_c$  and three spatial lattice sizes with  $N_s = 16, 20$  and  $24$  above  $T_c$ . The modes are counted with a bin size of 30 MeV below  $T_c$  and with a bin size of 50 MeV above  $T_c$ .

To study finite volume effects we have additionally generated ensembles of configurations on  $12^3 \times 6$ ,  $16^3 \times 6$  and  $24^3 \times 6$  lattices (see Table I). In Fig. 8 we compare our results for the topological susceptibility  $\chi_{top}$  obtained on all our lattices. One can see that the finite volume effects are rather small and unimportant for this observable. Finite lattice spacing effects seem to be also negligible,

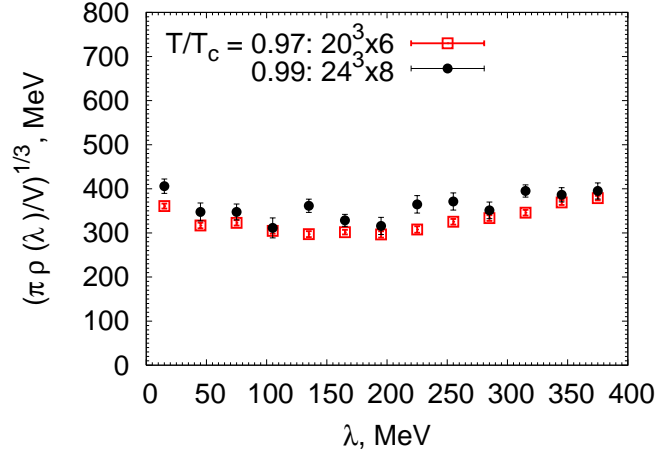


FIG. 10: The third root of the spectral density of non-zero eigenmodes of the overlap Dirac operator for two temperatures  $T < T_c$  closely approaching  $T_c$  on a  $20^3 \times 6$  and the  $24^3 \times 8$  lattice, respectively. The modes are counted with a bin size of 30 MeV.

since the  $\chi_{top}$  result on  $24^3 \times 8$  lattice is in accord with that on the  $20^3 \times 6$  lattice at the temperature where we have data available (see Fig. 8).

From Fig. 9 (left for  $T < T_c$  and right for  $T > T_c$ , restricted to the  $L > 0$  sector) we conclude, that the spectral density (if divided by the 4-volume) does not depend on the lattice volume for large  $\lambda$ , while some volume dependence is seen for  $\lambda \lesssim 100$  MeV for  $T < T_c$  (Fig. 9 left). Fig. 10 demonstrates a weak, if any, dependence of the spectral density in the confinement phase when the transition temperature is approached.

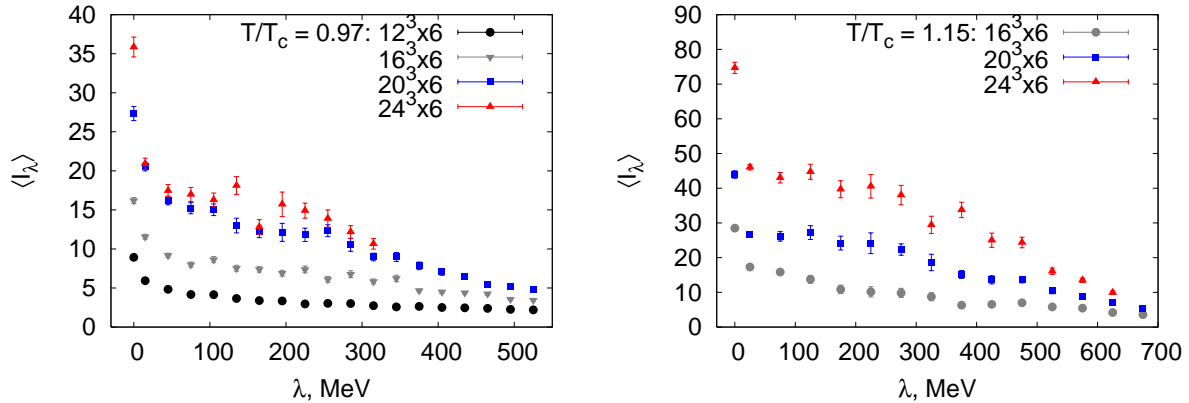


FIG. 11: The IPR averaged over zero modes and over spectral bins of width 30 MeV (left) and 50 MeV (right). Left: comparison for  $T = 0.97 T_c$  ( $N_\tau = 6$ ) between four spatial volumes with  $N_s = 12, 16, 20$  and  $24$ . Right: comparison for  $T = 1.15 T_c$  in the  $L > 0$  sector between three spatial volumes, on  $16^3 \times 6$ ,  $20^3 \times 6$  and  $24^3 \times 6$  lattices.

Coming now to the localization properties of the modes, we conclude from Fig. 11 that the IPR with increasing spatial volume increases (comparing lattice sizes from  $12^3 \times 6$  to  $24^3 \times 6$ ). This applies both to the confinement (left) and the deconfined (right) phases. In Fig. 12 we show, comparing the  $20^3 \times 6$  with the  $24^3 \times 8$  lattice (at approximately the same temperature and with a ratio of physical three-dimensional volumes of 0.86) that the lattice spacing effects are small. However, this is not the case for the zero modes. Their IPR nearly doubles when the lattice spacing  $a$  decreases by a factor

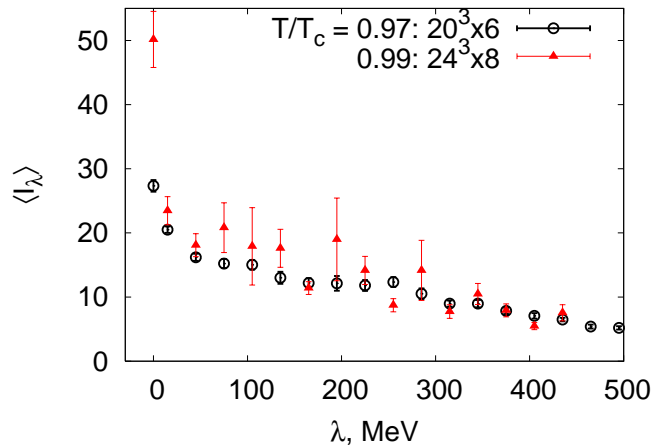


FIG. 12: The IPR averaged over zero modes and over spectral bins of width 30 MeV checked for lattice spacing effects by comparison between the  $20^3 \times 6$  lattice and the  $24^3 \times 8$  lattice for two temperatures  $T < T_c$  close to each other.

6/8. This corresponds to a dimensionality of the zero modes close to  $d \approx 2$  [20].

### IX. COMPARISON WITH EDWARDS *ET AL.*

As it has been said before, the overlap operator spectrum at finite temperature has been studied both in  $SU(2)$  and  $SU(3)$  gluodynamics by Edwards *et al.* [11]. In  $SU(2)$  case they made simulations at  $T/T_c = 1.0, 1.4$  and  $2.0$ . It has been found that for all temperatures considered the spectrum (for antiperiodic boundary conditions and positive Polyakov loop) consisted of two parts: a group of unexpected (and unobserved with staggered fermions!) near-zero modes, *i.e.* modes with small eigenvalues below  $0.05/a$  with a spectral density decreasing as a function of  $\lambda$ , and the rest with larger eigenvalues above  $0.05/a$  with a spectral density increasing with increasing  $\lambda$ . There was a large gap found between these two parts. The authors of Ref. [11] assumed that the small eigenvalues (the near-zero modes) are due to instanton-antiinstanton pairs and presented some evidence supporting this assumption. We prefer to call them more generally “topological objects” in what follows. In particular, Edwards *et al.* found that the number of small (near-zero) modes  $n_{sm}$ , combined with the number of zero modes  $n_0$ , is equal to the number of level crossings in the spectral flow of  $H_W$ , pointing towards a common origin. They stated that  $\langle Q^2 \rangle$  agreed well with the average  $\langle n \rangle$  where  $n = n_{sm} + n_0$ . We will find a similar remarkable agreement. Furthermore, it was found that the distribution of  $n = n_{sm} + n_0$  is in good agreement with a Poisson distribution

$$P(n; \langle n \rangle) = \frac{e^{-\langle n \rangle} \langle n \rangle^n}{n!}, \quad (10)$$

where  $\langle n \rangle$  is the ensemble average.

Our Fig. 4 (left) demonstrates that we have also observed the two parts of the eigenvalue spectrum mentioned above, although these two parts are not separated by a gap for  $T/T_c < 1.55$ , rather by a plateau of low spectral density. We therefore defined a boundary between the two parts of the spectrum for  $T/T_c < 1.55$  at 150 MeV which is approximately located at the minimum of the distribution  $\rho(\lambda)$ . We checked that all our results discussed below vary only within error bars when we vary this border value by 50 MeV.

Following the discussion in Ref. [11] we studied properties of  $\langle n \rangle$  and of the probability distribution

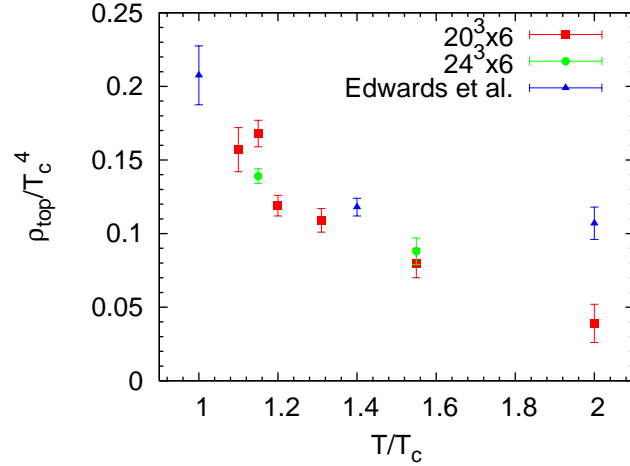


FIG. 13: The density of topological objects (see text) in units of  $T_c^4$  as a function of temperature  $T$ , from our data obtained for two 3-volumes at  $T > T_c$  and from the data of Ref. [11].

$P(n; \langle n \rangle)$  defined above. In Fig. 13 we present the density  $\rho_{top}$  defined as

$$\rho_{top} = \frac{\langle n \rangle}{V} \quad (11)$$

as a function of the temperature. For comparison, we show data from Ref. [11] which we took from their Table II. We computed the respective statistical errors by applying the bootstrap method to data collected there. We present in Fig. 13 our results for the  $24^3 \times 6$  lattice as well. There is good agreement between our results and results of Ref. [11] for smaller temperatures while data clearly disagree for the largest temperature  $T/T_c = 2.0$  [33]. One can see no essential volume dependence for this quantity which has been concluded by Edwards *et al.* as well. It is also seen that the density  $\rho_{top}$  is slowly decreasing with increasing temperature. The decrease with temperature is similar to that of the topological susceptibility. Numerically we indeed found nice agreement between  $\chi$  and  $\rho_{top}$  as can be seen from Fig. 14.

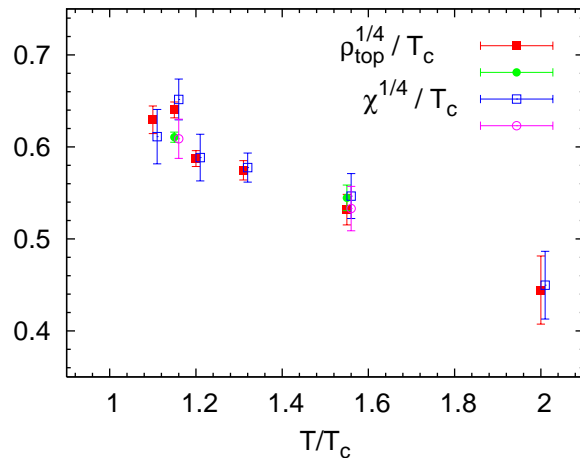


FIG. 14: Comparison of  $\rho_{top}^{1/4}/T_c$  (full symbols) and  $\chi^{1/4}/T_c$  (empty symbols) for  $20^3 \times 6$  (squares) and  $24^3 \times 6$  (circles) lattices.

In Fig. 15 the ratio  $\langle n \rangle / D$  is depicted, where  $D$  is the variance of the multiplicity  $n$  of topological objects including near-zero and zero modes. For the Poisson distribution exactly  $\langle n \rangle = D$  holds. One can see that our results agree with this equality except for one data point. Thus we confirm the earlier observation of Ref. [11] that the distribution of  $n$  is consistent with the assumption of mutual independence between the respective topological objects.

In Fig. 16 we show the ratio  $\langle n_{sm} \rangle / \langle n \rangle$  which indicates how the contribution of the near-zero (small eigenvalue) modes to all topological objects changes with volume and eventually with temperature. At two temperatures,  $T/T_c = 1.15$  and  $T/T_c = 1.55$ , where we are in the position to compare two three-dimensional volumes ( $N_s = 20$  and  $N_s = 24$  with the same  $N_\tau = 6$ ) we could find this ratio rising with the volume. In other words, the larger the three-dimensional volume, the more near-zero modes exist compared to the zero modes. This behavior is consistent with a binomial distribution proposed in Ref. [11] for topological objects with positive and negative charge, with  $n_0 = |n_+ - n_-|$  zero modes and  $n_{sm} = 2 \min(n_+, n_-)$  near-zero modes. On the other hand, the share of near-zero modes among all topological objects seems to decrease with increasing temperature. One should have in mind that the physical spatial volume in our setting rapidly decreases (like  $(N_s / (N_\tau T))^3$ ) with increasing temperature. For  $T/T_c > 1.2$  the ratio is already less than one half, indicating that the volumes are already so small that the total multiplicity is suppressed such that there are more zero modes than near-zero modes.

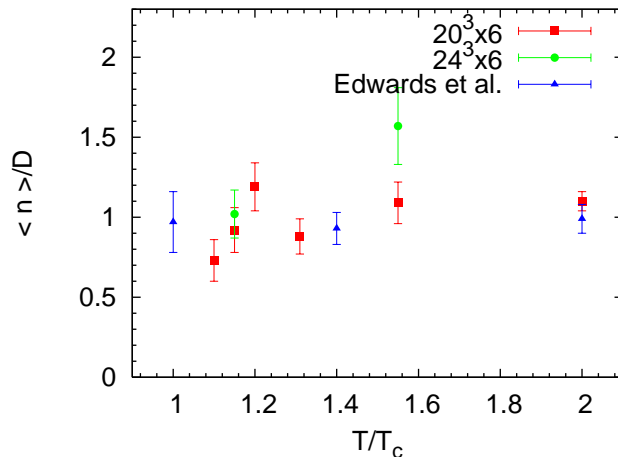


FIG. 15: The ratio of the average number of all topological objects  $\langle n \rangle$  to its variance as a function of temperature  $T$ , from our data obtained for two 3-volumes at  $T > T_c$  and from the data of Ref. [11].

Now let us look at the problem of the spectral gap taking into account the existence of a separate part of near-zero eigenvalues in the spectrum as discussed above. Alternatively to the definition of the spectral gap used in section VI one can consider a definition  $\bar{g}_\lambda$  which takes into account only the bulk non-zero modes in the spectrum, thus ignoring the small non-zero eigenvalues (near-zero modes) altogether. This alternative definition can be applied to our data at  $T/T_c = 1.55$ , a temperature at which we observe a clear gap between near-zero and larger eigenvalues. In the left panel of Fig. 17 we show the dependence of the conventional spectral gap, as defined in section VI, on the inverse lattice size for two temperatures in the case of  $L > 0$ . The general tendency of a spectral gap is decreasing with increasing volume. The interesting question is whether it has an infinite-volume limit different from zero. One can see that for  $T/T_c = 1.15$  the spectral gap decreases very steeply with increasing volume, starting from values like  $g_\lambda \approx 300 \dots 400 \text{ MeV}$  on lattices of size  $L \sim 1.4 \text{ fm}$ . The gap is already less than 100 MeV for  $L > 2.2 \text{ fm}$ , eventually turning to zero in the infinite-volume limit. At higher temperature,  $T/T_c = 1.55$ , we also see that the “old” gap  $g_\lambda$  decreases with increasing volume, although not so fast. Still, we cannot exclude that the fate of the spectral gap is the same at the higher temperature.

Thus, the old definition of the spectral gap gives some support to the conclusion made in Ref. [11]

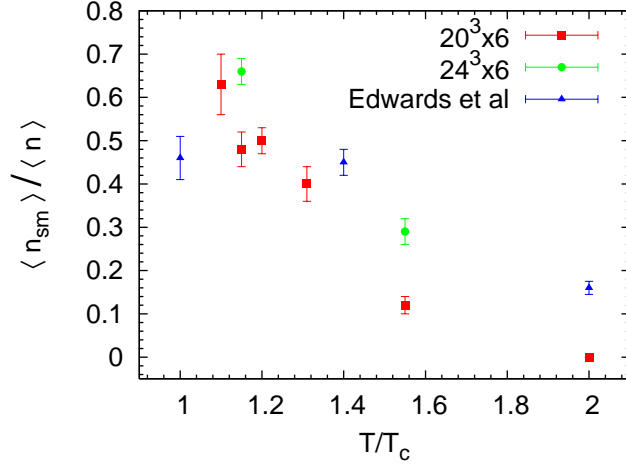


FIG. 16: The ratio of the average number of small non-zero modes  $\langle n_{sm} \rangle$  to the average number of all topological objects  $\langle n \rangle$  as a function of temperature  $T$ , from our data obtained for two 3-volumes at  $T > T_c$  and from the data of Ref. [11].

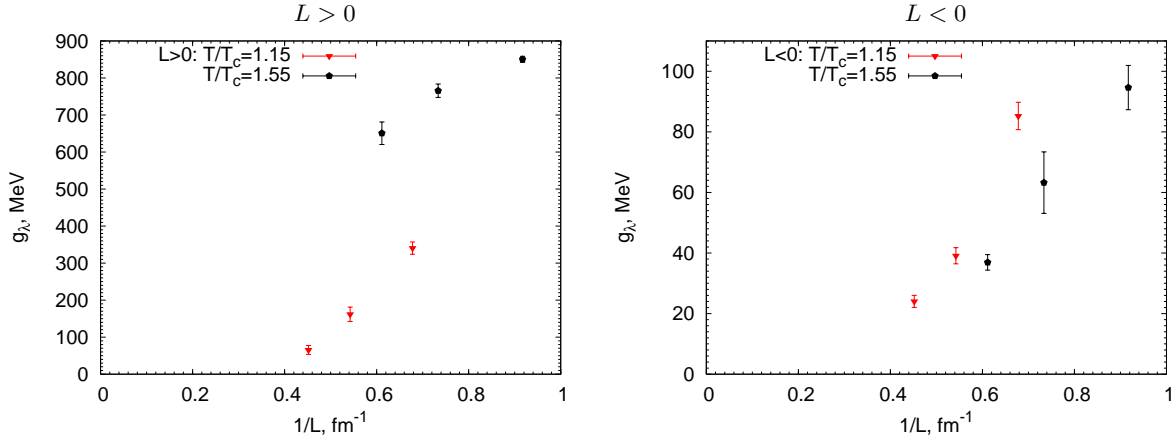


FIG. 17: The spectral gap  $g_\lambda$  as defined in section VI vs. inverse lattice size for  $T/T_c = 1.15$  and  $T/T_c = 1.55$ , separated according to the sign of the averaged Polyakov loop  $L > 0$  (left) and  $L < 0$  (right).

that in the deconfinement phase of  $SU(2)$  gluodynamics the chiral condensate is nonzero, at least up to some specific temperature, even in the  $L > 0$  sector.

In the right panel of Fig. 17 the conventional spectral gap  $g_\lambda$  is also shown for  $L < 0$ . Compared to the case of  $L > 0$ , the spectral gap for  $L < 0$  is much smaller. There is a clear tendency for  $g_\lambda$  at  $L < 0$  steeply to decrease with increasing volume. Data in Fig. 17(right) suggest that the dependence of  $g_\lambda$  on  $1/L$  is  $1/L^\gamma$  with  $\gamma > 1$ . Our rough estimation results in  $\gamma \approx 3$ . To make a more precise statement we need new data points for bigger volumes. The same is valid for the data set at  $T/T_c = 1.15$  for  $L > 0$  shown in the right panel of Fig. 17.

For the same physical 3-volume, the gap increases with increasing temperature only in the case of  $L > 0$ . For the negative Polyakov loop sector the tendency is reverse, corresponding to the increasing spectral density.

Let us now turn to Fig. 18 where results for the “new” definition  $\bar{g}_\lambda$  of the spectral gap, excluding the small eigenvalues of the near-zero modes, are presented. Now we see a strong indication for a convergence of the spectral gap  $\bar{g}_\lambda$  to a finite intercept at  $1/L = 0$  for both temperatures. Note that

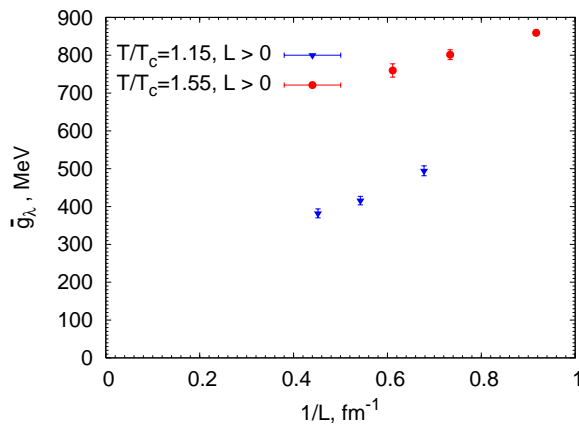


FIG. 18: The “new” spectral gap  $\bar{g}_\lambda$  for  $L > 0$ , as defined in section IX with exclusion of the near-zero modes, is shown vs. inverse lattice size for  $T/T_c = 1.15$  and  $T/T_c = 1.55$ .

for  $T/T_c = 1.15$  only eigenvalues  $\lambda < 120$  MeV have been excluded in this way, a value substantially below the value of the new emerging gap. Thus, excluding the near-zero modes leads to a definition of the spectral gap  $\bar{g}_\lambda$ , such that it stays non-zero in the limit  $V \rightarrow \infty$  for  $L > 0$  at both temperatures  $T > T_c$ .

Summarizing our findings presented in this section we confirm the existence, at  $T > T_c$ , of particular modes with small non-zero eigenvalues which are most probably related to topological objects, similar to the zero modes. So it is natural to consider them separately from the other (bulk) non-zero modes. We are planning to enter a further study of their properties in the near future.

## X. COMPARISON WITH T=0

The details of simulations at zero temperature are presented in Table I. The lattice coupling and the lattice size were chosen in such a way that the physical box size was kept approximately fixed and equal to 1.4 fm. In Fig. 19 we show results for the topological susceptibility as a function of the lattice spacing squared. The linear fit results in  $\chi^{1/4} = 202(5)$  MeV. This number is in good agreement with earlier results obtained with various gluonic definitions of the topological charge on lattices generated with the Wilson action. It also agrees well with our results for  $T < T_c$ . Comparing Fig. 19 with the results for the Wilson action [19], obtained using the same method to compute the topological charge as applied in the present paper, we see that the scaling properties are better for the tadpole-improved Symanzik action.

In Fig. 20 the spectral density as obtained on the  $14^4$  lattice for  $\beta_{\text{imp}} = 3.281$  is shown. This coupling value is close to one value ( $\beta_{\text{imp}} = 3.275$ ) used in the finite temperature simulations at  $T \sim T_c$ . One can see that the spectral density in Fig. 20 is in good agreement with that shown in Fig. 3 except for the lowest interval  $\lambda < 100$  MeV. For  $T = 0$ , we do not see in this range of  $\lambda$  the increase of  $\rho(\lambda)$  with  $\lambda \rightarrow 0$  that was observed approaching  $T \rightarrow T_c$  from below. Comparing with the respective result for the Wilson action [19] we see good agreement.

We have also measured the IPR for zero temperature. The results are presented in Fig. 21. The results are again in full agreement with those of Ref. [19]. Comparing the  $T = 0$  results with our observations at  $T < T_c$  (see Fig. 6) at approximately equal  $\beta_{\text{imp}}$ , we see an essential difference: at non-zero temperature the IPR close to  $\lambda = 0$  is substantially higher.



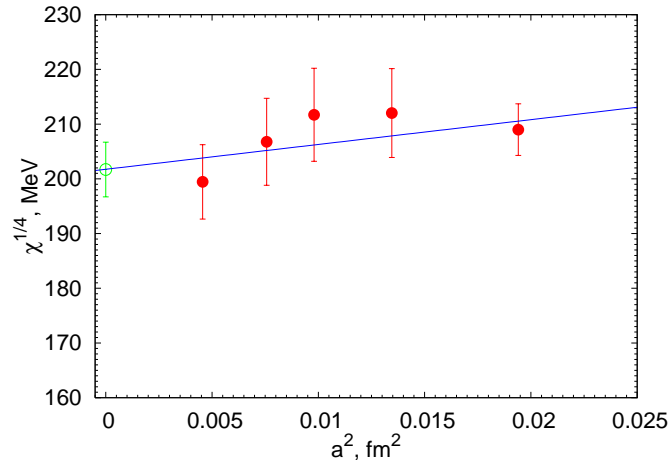


FIG. 19: The fourth root of the topological susceptibility at  $T = 0$  as function of the lattice spacing  $a$ . The empty circle shows the result of the linear extrapolation to  $a = 0$ .

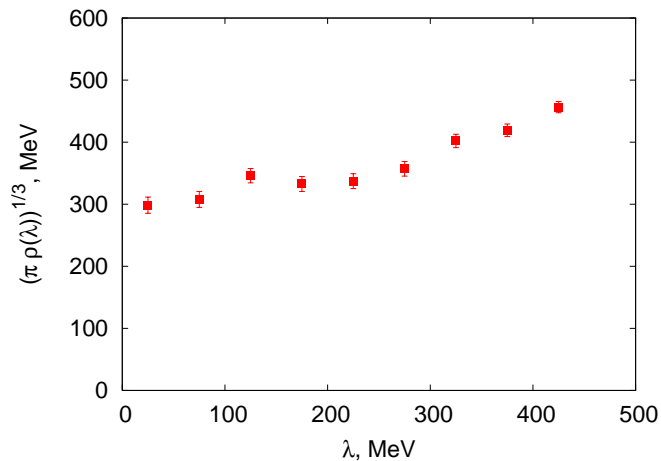


FIG. 20: The spectral density obtained on the  $14^4$  lattice with  $\beta = 3.281$ . The modes are counted with a bin size of 50 MeV.

## XI. SUMMARY

After a first overlap study of topological aspects of  $SU(2)$  pure gauge theory at finite temperature [11], based on the Wilson gauge field action, we returned to these topics. We have performed measurements of the topological susceptibility, the spectral density and the localization properties of fermionic eigenmodes with the help of the overlap Dirac operator in finite temperature  $SU(2)$  gluodynamics, simulated with the tadpole-improved Symanzik action. We found that the topological susceptibility in the confinement phase is almost independent of temperature. It starts slowly to decrease in the deconfinement phase, in agreement with previous results [16] which were obtained with the Wilson gauge field action and an improved gluonic definition of the topological charge density. In contrast to the other quantities, we did not find systematic effects of the sign of the averaged Polyakov loop on the topological susceptibility.

While these results (see Sect. IV) could have been expected, the remaining observations concerning the spectral properties might come as a surprise, if not at a qualitative then at a quantitative level.

Assuming antiperiodic boundary conditions for the fermionic fields throughout this paper we have

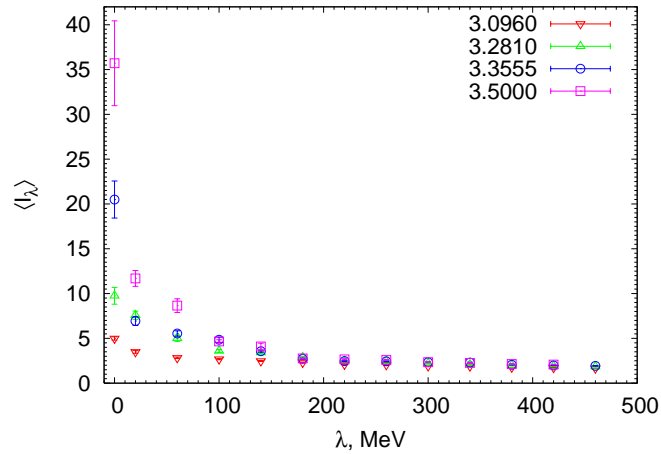


FIG. 21: The IPR averaged over zero modes and over subsequent spectral bins of width 30 MeV at  $T = 0$  for four different  $\beta$ -values .

discussed the behavior of the chiral condensate defined via the Banks-Casher relation below and above the phase transition. A qualitatively different behavior of the spectral density has been observed at  $T > T_c$  for ensembles having opposite sign of the Polyakov loop  $L$  (see Sect. V). The spectral density is decreasing with rising temperature for  $L > 0$  until it is finally disrupting around  $T \sim 1.5 T_c$ . On the other hand, for  $L < 0$  the density begins to rise with increasing temperature.

Although the spectral gap  $g_\lambda$ , defined as the average of the lowest non-zero eigenvalue, as a function of temperature shows qualitative agreement with respective data for  $SU(3)$  gauge theory (see Fig. 5) we observed that the respective volume dependence is completely different. We found that  $g_\lambda$  tends fast to zero with increasing volume for  $L > 0$  at  $T/T_c = 1.15$  and for  $L < 0$  for both  $T/T_c = 1.15$  and 1.55 in contrast to the situation in  $SU(3)$  where a rather weak volume dependence of the gap was observed in both real and complex  $L$  sectors.

Increasing of the gap  $g_\lambda$  with increasing temperature for  $L > 0$  and fixed lattice size is explained by the strong volume dependence of the number of near-zero modes as can be seen from Fig. 16. We are making measurements on the lattice, with  $N_s = 20$  defining its physical size, which decreases with increasing temperature, resulting in a decreasing number of near-zero modes. The consequence is that not each lattice configuration has these modes. This in turn makes the *ensemble average*  $g_\lambda$  to increase with temperature.

The localization properties of the eigenmodes have been investigated in terms of the inverse participation ratio (IPR), and the dependence of the average IPR on volume and discretization has been monitored all over the lower part of the spectrum (see Sect. VII). We repeat here only two remarkable facts. At first, sizeable lattice spacing effects have been found only for the zero modes (close to  $T_c$ ) which is pointing to a dimensionality  $\approx 2$ . Second, at  $L < 0$ , the eigenmodes responsible for the non-vanishing chiral condensate above  $T_c$ , that are filling the region up to  $\lambda \sim 400$  MeV, are very delocalized compared to the isolated modes that exist in that spectral range for  $L > 0$ .

Special considerations have been devoted in Sect. IX to the near-zero modes found in the subensemble with  $L > 0$ . The spectral density has been divided into an interval with small eigenvalues and the rest with all larger eigenvalues, motivated by the observation that for large enough temperatures  $T \approx 1.5 T_c$  these two parts of the spectrum become well separated, whereas a small number of near-zero modes still exists. The topological susceptibility (which had been defined through the total topological charge  $Q$  obtained by counting the zero modes alone) now has been compared with the density of topological objects defined *including* the near-zero modes. Good agreement was found. This justifies the dilute-gas approximation,  $\chi = \rho_{top}$  with charge  $Q \approx \pm 1$  objects. This is corroborated by the observation that the multiplicity of all topological objects follows the Poisson distribution

with reasonable accuracy as indicated by Fig. 15 and was reported earlier in Ref. [11]. Further, the percentage of near-zero modes among the lower part of the spectrum (*i.e.* including also the true zero-modes) has been measured for different temperatures and volumes, see Fig. 16. It was found to rise with increasing volume, and the apparent temperature suppression observed in our measurements might be mainly explained as a volume effect.

Based on all these observations, emphasizing the special role of the near-zero modes, an alternative definition of the spectral gap  $\bar{g}_\lambda$  *excluding* the near-zero modes has been proposed. Following this definition, a non-vanishing infinite-volume limit of  $\bar{g}_\lambda$  in the deconfined phase *at all temperatures*  $T > T_c$  now seems possible for the  $L > 0$  sub-ensemble, in clear distinction to the other definition and, as we have seen, to the  $L < 0$  sub-ensemble. Then we end up with an unusual situation in the temperature interval  $T_c < T < 2 T_c$ : a finite density of the near-zero modes coexists with a gap between these modes and the bulk of the spectrum. Whether we really may speak about broken chiral symmetry depends on a nonvanishing infinite-volume limit of the spectral density  $\rho_{sm}(\lambda)$  at  $\lambda = 0$ . Otherwise we could ignore the presence of the near-zero modes for this question and consider the new definition  $\bar{g}_\lambda$  of the spectral gap as a proper one. In any case, more studies of the thermodynamical limit are necessary in order to confirm or reject the possibility to reconcile, in that limit, the restoration of chiral symmetry,  $\rho(\lambda = 0) = 0$ , with a gap  $g_\lambda \rightarrow 0$ . [34]

It shall be noted that by now, the “kinematic” understanding for the relation between chiral symmetry breaking (and restoration) and the sign of an eventually nonzero value of the Polyakov loop (or, equivalently, on the change of the boundary conditions in the Dirac operator) is much more developed than at the time when our study was begun [5].

A series of papers [26, 27, 28, 29, 30] discusses the connection between the spectrum of a (fairly general) Dirac operator and the breaking of center symmetry, *i.e.* the emergence of a nonvanishing Polyakov loop. The most concise quantity in this respect is the “dual quark condensate” defined in Ref. [29], the Fourier transform of the standard quark condensate

$$\Sigma = \frac{1}{V} \langle \text{Tr} [(m + D_\phi)^{-1}] \rangle$$

with respect to the angle  $\phi$  modifying the boundary condition of the Dirac operator  $D_\phi$ . A “fat Polyakov loop” formed out of singly wrapped paths is obtained as the lowest ( $n = 1$ ) Fourier component. Higher Fourier components correspond to multiply wrapped Polyakov loops. The condition for a nonvanishing “fat” Polyakov loop is a nonvanishing periodic component  $\propto \cos(\phi)$  in the fermionic spectral density, in other words, a nontrivial response of the spectral density to the change of the boundary conditions.

A microscopic explanation of the onset of such a sensitivity of the Dirac spectrum to the type of boundary conditions in the context of a nonvanishing Polyakov loop of either sign needs to be worked out. What comes to mind is the interplay of holonomy and topology of dyons [9]. This difference is accompanied by a different localization behavior of the lowest fermionic eigenmodes in the two sectors.

### Acknowledgements

The work of ITEP group is partially supported by RFBR grants RFBR 08-02-00661a and RFBR 07-02-00237a, by the grant RFBR 06-02-04010-NNIOa together with the DFG grant 436 RUS 113/739/2, and the grant for scientific schools NSH-679.2008.2. A considerable part of the computations has been performed on the MVS 50K multiprocessor system at the Moscow Joint Supercomputer Center.

The work of E.-M. I. was supported by DFG through the Forschergruppe FOR 465 (Mu932/2). We thank Maxim Chernodub and Christof Gattringer for discussions on an earlier version. E.-M. I. is grateful to the Karl-Franzens-Universität Graz for the guest position he holds while the revised version is written up.

- 
- [1] M. A. Stephanov, Phys. Lett. **B 375** (1996) 249 [hep-lat/9601001].
- [2] S. Chandrasekharan and N. Christ, Nucl. Phys. Proc. Suppl. **47** (1996) 527 [hep-lat/9509095].
- [3] S. Chandrasekharan, Dong Chen, N. Christ, W. Lee, R. Mawhinney, and P. Vranas, Phys. Rev. Lett. **82** (1999) 2463 [hep-lat/9807018].
- [4] Ch. Gattringer, P. E. L. Rakow, A. Schäfer, and W. Söldner, Phys. Rev. **D 66** (2002) 054502 [hep-lat/0202009].
- [5] V. G. Bornyakov, E. V. Luschevskaya, S. M. Morozov, M. I. Polikarpov, E.-M. Ilgenfritz, and M. Müller-Preussker, PoS LAT2007 (2007) 315 [arXiv:0710.2799 (hep-lat)].
- [6] H. Neuberger, Phys. Lett. **B 417** (1998) 141 [arXiv:hep-lat/9707022].
- [7] P. Hasenfratz, V. Laliena, and F. Niedermayer, Phys. Lett. **B427** (1998) 125 [hep-lat/9801021].
- [8] D. H. Adams, J. Math. Phys. **42** (2001) 5522 [hep-lat/0009026].
- [9] V. G. Bornyakov, E.-M. Ilgenfritz, B. V. Martemyanov, S. M. Morozov, M. Müller-Preussker, and A. I. Veselov, Phys. Rev. **D 76** (2007) 054505 [arXiv:0706.4206 (hep-lat)].
- [10] F. Niedermayer, Nucl. Phys. Proc. Suppl. **73** (1999) 105 [hep-lat/9810026].
- [11] R. G. Edwards, U. M. Heller, J. E. Kiskis, and R. Narayanan, Phys. Rev. **D 61** (2000) 074504 [arXiv:hep-lat/9910041].
- [12] V. G. Bornyakov, E.-M. Ilgenfritz, and M. Müller-Preussker, Phys. Rev. **D 72** (2005) 054511 [hep-lat/0507021].
- [13] J. Engels, J. Fingberg, and M. Weber, Nucl. Phys. **B 332** (1990) 737.
- [14] ARPACK source: <http://www.caam.rice.edu/software/ARPACK/>
- [15] Ch. Gattringer and R. Pullirsch, Phys. Rev. **D 69** (2004) 094510 [hep-lat/0402008].
- [16] B. Alles, M. D'Elia, and A. Di Giacomo, Phys. Lett. **B 412** (1997) 119 [hep-lat/9706016].
- [17] T. Banks and A. Casher, Nucl. Phys. **B 169** (1980) 103.
- [18] E.-M. Ilgenfritz, K. Koller, Y. Koma, G. Schierholz, T. Streuer, and V. Weinberg, Phys. Rev. **D 76** (2007) 034506 [arXiv:0705.0018 (hep-lat)].
- [19] F. V. Gubarev, S. M. Morozov, M. I. Polikarpov, and V. I. Zakharov, JETP Lett. **82** (2005) 343, Pisma Zh. Eksp. Teor. Fiz. **82** (2005) 381 [hep-lat/0505016].
- [20] Y. Koma, E.-M. Ilgenfritz, K. Koller, G. Schierholz, T. Streuer, and V. Weinberg, PoS LAT2005 (2006) 300, [hep-lat/0509164].
- [21] V. Weinberg, E.-M. Ilgenfritz, K. Koller, Y. Koma, G. Schierholz, and T. Streuer, PoS LAT2006 (2006) 078, [hep-lat/0610087].
- [22] V. Weinberg, E.-M. Ilgenfritz, K. Koller, Y. Koma, G. Schierholz, and T. Streuer, PoS LAT2005 (2006) 171, [hep-lat/0510056].
- [23] V. Weinberg *et al.* (DIK Collaboration), PoS LAT2007 (2007) 236, [arXiv:0710.2565 (hep-lat)].
- [24] Ch. Gattringer, M. Göckeler, P.E.L. Rakow, St. Schaefer, and A. Schäfer, Nucl. Phys. **B 617** (2001) 101 [hep-lat/0107016].
- [25] Ch. Gattringer, M. Göckeler, P.E.L. Rakow, St. Schaefer, and A. Schäfer, Nucl. Phys. **B 618** (2001) 205 [hep-lat/0105023].
- [26] Ch. Gattringer, Phys. Rev. Lett. **97** (2006) 032003 [hep-lat/0605018].
- [27] F. Bruckmann, Ch. Gattringer, and Ch. Hagen, Phys. Lett. **B 647** (2007) 56 [hep-lat/0612020].
- [28] Ch. Hagen, F. Bruckmann, E. Bilgici, and Ch. Gattringer, PoS LAT2007 (2007) 289, [arXiv:0710.0294 (hep-lat)].
- [29] E. Bilgici, F. Bruckmann, Ch. Gattringer, and Ch. Hagen, Phys. Rev. **D 77** (2008) 094007 [arXiv:0801.4051 [hep-lat]].
- [30] F. Synatschke, A. Wipf, and K. Langfeld, Phys. Rev. **D 77** (2008) 114018 [arXiv:0803.0271 [hep-lat]].
- [31] We stress, however, that this property is not guaranteed for lower  $\beta$  and for the Wilson action [9].
- [32] Of course, our results imply that to calculate the topological susceptibility one could average over all Polyakov loop sectors.
- [33] For this temperature there is a discrepancy with the results of Ref. [11] also in the case of the topological susceptibility.
- [34] We thank one of the anonymous referees for pointing out to us such a scenario.